Particle Sizing and Spray Analysis

Norman Chigier, Gerald W. Stewart
Chairmen/Editors

1985

Proceedings of SPIE—The International Society for Optical Engineering

Volume 573

Particle Sizing and Spray Analysis

Norman Chigier, Gerald W. Stewart
Chairmen/Editors

Cooperating Organizations
Optical Sciences Center/University of Arizona
Institute of Optics/University of Rochester

August 21, 1985
San Diego, California

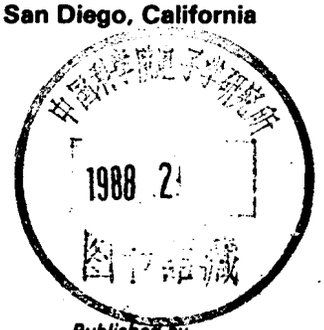

Published by
SPIE—The International Society for Optical Engineering
P.O. Box 10, Bellingham, Washington 98227-0010 USA
Telephone 206/676-3290 (Pacific Time) • Telex 46-7053

Please use the following format to cite material from this book:
Author(s), "Title of Paper," *Particle Sizing and Spray Analysis,* Norman Chigier, Gerald W. Stewart, Editors, Proc. SPIE 573, page numbers (1985).

Library of Congress Catalog Card No. 85-062842
ISBN 0-89252-608-4

Printed in the United States of America.

PARTICLE SIZING AND SPRAY ANALYSIS

Volume 573

Conference Committee

Chairmen
Norman Chigier
Carnegie-Mellon University

Gerald W. Stewart
Aerodyne Research, Incorporated

Program Committee

William D. Bachalo
Aerometrics, Incorporated

E. Dan Hirleman
Arizona State University

Brian J. Thompson
University of Rochester

Session Chairman

Session 1—Particle Sizing and Spray Analysis
William D. Bachalo, Aerometrics, Incorporated

Volume 573

INTRODUCTION

Particle field measurements are of interest over a vast and diverse range of applications. The need to obtain accurate measurements of particle size distributions, veolcities and concentration is associated with monitoring pollutant emissions, evaluating and improving combustion, meteorological investigations, agricultural applications, including irrigation and pesticide dispersal, and innumerable industrial applications. In the electronics industry, the presence of particles in clean rooms must be carefully monitored since minute amounts of contaminants can cause failures, for example, in integrated circuits and disk drives. Recent research and development primarily in the optical methods have addresed these recognized needs for satisfactory diagnostics.

Whether seeking a method for possible commercial development or selecting an instrument to fulfill certain measurement requirements, a number of selection criteria need to be considered. Perhaps of first importance is the anticipated particle size range to be measured. Light scatter detection methods can detect a wide range of particle sizes from submicron to several millimeters in diameter. Imaging methods are limited to particles larger than approximately 5 microns. The particle morphology is also an important parameter to be considered. For example, some light scatter detection methods are relatively insensitive to particle shape or composition whereas others can produce erroneous results. In general, imaging methods have the capability of determining the shape of large particles and obtain size determinations independent of the particle composition. However, the automation of the image analysis remains as a serious limitation.

Optical methods currently in use or under development generally perform the measurements in situ and nonintrusively. Over the past decade, sampling methods have been shown to be unreliable and are used only when no other alternative exists. Some optical methods are semi-intrusive. That is, the optical probe has a limited working range and, thus, must be inserted into the process being measured. Such methods also present questions regarding the biasing produced by the disturbance to the flow field.

Recent research and development in particle sizing instrumentation has placed notable emphasis on the parallel developments in lasers, electronics, microprocessors, and computers. This is especially true of the light scatter detection methods. Light scattering codes can be run on personal computers at insignificant cost. Hence, the effects of the various scattering parameters may be investigated in detail. In the implementation of the methods, state-of-the-art electronics have been used to increase the accuracy, speed and dynamic range of the signal processors. Personal computers serve to provide convenience and speed in data management and storage. The use of signal validation logic developed in the software is providing greater accuracy and confidence in the measurements.

The papers given in this proceedings volume describe some of the recent developments in the particle sizing technology. Both imaging and light scatter detection methods are described. It is significant that meaningful comparisons of results obtained by different methods were presented. For one who has worked in this area for a number of years and has endured some of the attendant frustrations and disappointments, the presentation of measurements in realistic environments and the agreement in the results is most encouraging.

William D. Bachalo
Aerometrics, Inc.

PARTICLE SIZING AND SPRAY ANALYSIS

Volume 573

Contents

PARTICLE SIZING AND SPRAY ANALYSIS

Volume 573

Session 1

Particle Sizing and Spray Analysis

Chairman
William D. Bachalo
Aerometrics, Incorporated

Obtaining particle velocity and displacement distributions from double-exposure holograms using optical and digital processing

P. H. Malyak, B. J. Thompson

The Institute of Optics, College of Engineering and Applied Science
University of Rochester, Rochester, NY 14627

Abstract

A double-exposure far-field hologram contains particle displacement and velocity information for all particles within a given sample volume. The optical Fourier transform of such a hologram contains a set of fringes which are dependent on the probability density function (pdf) that characterizes the distribution of particle displacements or velocities. It is demonstrated that intensity data measured in the transform plane of a doubly exposed hologram may be processed to yield this pdf for particle motion in one dimension. In the 2-dimensional case, the marginal pdf's may be obtained when the orthogonal components of displacement are independent. Experimental results for 1- and 2-dimensional distributions are presented and good agreement between theory and experiment is observed.

Introduction

Far-field holography has been used extensively over the past 20 years for counting and sizing small particles. The first practical application involved the study of naturally occurring fog droplets having a range in size from 4μm to 200μm.[1,2] Since the initial application, a wide variety of particle fields have been analyzed holographically including aerosols, marine plankton and gas bubbles in liquids. The literature describing holographic particle analysis is rather extensive and has been reviewed on several occasions;[3-6] the references contained in these articles provide a reasonably complete bibliography of the field up to 1982. From 1982 to the present, new results and applications have continued to appear in the literature (see, e.g., Ref. 7-10).

A natural extension of the holographic technique is to record a double-exposure hologram of a dynamic particle sample so that particle velocity information may be obtained.[3] Clearly, each particle in the sample volume will produce two images when the double-exposure hologram is reconstructed. Hence, measuring the displacement between the image-pairs related by translation and dividing by the time interval between exposures will yield the velocities of the individual particles.

Manual readout of both single-exposure and double-exposure holograms can become tedious and time-consuming when the sample consists of a large number of particles. As a result, there is a need for automated readout. One technique for automated readout involves the use of digital image processing to obtain the required data from the holographic reconstruction of the particle sample. The apparatus used for digital readout typically includes a TV camera, an image digitizer, an x-y-z translator on which the hologram (or TV camera) is mounted and, of course, a computer. The reconstructed sample volume is scanned automatically by operating the translator under computer control while the image digitizer allows the computer to "see" that portion of the reconstruction which is imaged onto the vidicon. Individual particle images will go in and out of focus as the sample volume is scanned; hence, it is necessary to include software that allows the computer to determine when a particle image is brought into focus. Once the particle image is in focus, the computer can be used to obtain the parameters of interest, i.e., particle size, position and displacement. A number of authors have successfully applied digital readout methods in the analysis of particle field holograms. For example, Bexon et al.[11] describe a system, based on the Quantimet 720 Image Analyzing Computer, for measuring the size and position of the particle images obtained from an in-line far-field hologram. Payne et al.[12] applied digital analysis to obtain particle velocities from a sequence of far-field holograms. The size, shape and position of the particle images from each hologram were determined with the help of a computer. The particle displacements were then obtained by tracking the individual particle images from frame to frame.

Another method of automated readout, first reported by Ewan,[13,14] involves forming the optical Fourier transform of a doubly exposed far-field hologram. The intensity data measured in the transform plane is then processed digitally to yield the particle velocity information. The optical-digital (or hybrid) system described by Ewan is fundamentally different from the digital approach described above. Whereas the displacements of the particles are individually computed when using the digital technique, the hybrid system allows the distribution of displacements to be determined without directly considering the

individual particle displacements. As a result, the hybrid system is inherently faster than the digital readout method when the sample contains a large number of particles. A further advantage of the hybrid system, as compared to the manual and digital readout methods, is that it is not required to determine which particle image-pairs are related by translation. (Pairing up the images can be difficult when the number density of particles is large.) Since the operation of the hybrid readout system depends on the autocorrelation function of the composite particle field,[13] the velocity distribution may be obtained without having to determine which image-pairs are related by translation.

In this paper, the properties of the optical Fourier transform of a double-exposure far-field hologram are briefly reviewed. An algorithm is then developed for obtaining the probability density function (pdf) that characterizes the distribution of particle displacements for the 1-dimensional case. Measuring 2-dimensional particle displacements is also addressed and experimental results are presented.

The optical Fourier transform of a double-exposure far-field hologram

The configuration used for recording an in-line far-field hologram is shown in Fig. 1a. For the purpose of illustration, the object shown consists of a single particle that is illuminated with a collimated beam of coherent light. The recording (or hologram) plane is located a distance z away from the object where z satisfies the far-field condition (i.e., $z >> d^2/\lambda$ where d denotes the particle diameter and λ is the wavelength of the incident beam).

The Fourier transform of the doubly exposed hologram is obtained optically as shown in Fig. 1b. It may be shown that the expected value of the intensity in the transform plane $\langle I_F(u,v)\rangle$ is given by[15]

$$\langle I_F(u,v)\rangle = |\tilde{A}(\tfrac{u}{\lambda f}, \tfrac{v}{\lambda f})|^2 \cos^2 \frac{\pi z(u^2+v^2)}{\lambda f^2} \sum_{n=1}^{N} [1 + \cos \tfrac{2\pi}{\lambda f}(u\Delta\xi_n + v\Delta\eta_n)], \qquad (1)$$

where u and v are the coordinates in the transform plane, λ denotes the wavelength of the illuminating beam, f is the focal length of the transform lens, z is the object-to-hologram separation and N is the total number of particles in the sample. In obtaining the above expression, it was assumed, for simplicity, that all particles in the sample are located in the ξ,η-plane. The horizontal and vertical components of particle displacement are represented by $\Delta\xi_n$ and $\Delta\eta_n$, respectively. It was also assumed that the particles of interest are opaque, in which case, the quantity $\tilde{A}(\cdot)$ represents the Fourier transform of $A(\xi,\eta)$ where $A(\xi,\eta)$ describes the cross-sectional shape of a typical particle. As indicated by the summation term in Eq. (1), each particle image-pair related by translation contributes a set of cosinusoidal fringes of a particular frequency to the total diffraction pattern. The fringe frequency and orientation are directly related to the magnitude and direction, respectively, of the displacement of a given particle.

Typically, the particle displacements in Eq. (1) are random and may be characterized in terms of a probability density function $p(s_1,s_2)$. For a large number of particles, the summation term in Eq. (1) may be approximated by an integral involving $p(s_1,s_2)$, i.e.,

$$\langle I_F(u,v)\rangle = I_0(u,v)\{1 + \int_{-\infty}^{\infty}\int p(s_1,s_2) \cos[\tfrac{2\pi}{\lambda f}(us_1 + vs_2)]\, ds_1 ds_2\}, \qquad (2)$$

where

$$I_0(u,v) = |\tilde{A}(\tfrac{u}{\lambda f}, \tfrac{v}{\lambda f})|^2 \cos^2(\frac{\pi z p^2}{\lambda f^2}). \qquad (3)$$

If the particle motion is confined to one direction, a 1-dimensional pdf $p(s_1)$ will be sufficient to describe the distribution of displacements. Thus the intensity in the transform plane may be written as

$$\langle I_F(u,v)\rangle = I_0(u,v)\{1 + \int_{-\infty}^{\infty} p(s_1) \cos(\frac{2\pi u s_1}{\lambda f})\, ds_1\}. \qquad (4)$$

To illustrate how a distribution of displacements affects the transform pattern, it is helpful to consider a specific distribution. For example, if the distribution of displacements is characterized by a Gaussian pdf, the intensity in the transform plane is

given by

$$\langle I_F(u,v)\rangle = I_0(u,v)\{1 + \exp[-\frac{2\pi^2\sigma^2u^2}{\lambda^2f^2}]\cos(\frac{2\pi\mu u}{\lambda f})\}\ , \qquad (5)$$

where μ denotes the mean displacement and σ denotes the standard deviation. The above expression indicates that a set of cosinusoidal fringes are present in the transform plane where the fringe frequency is determined by the mean particle displacement. It is observed that the cosine term in Eq. (5) is modulated by an exponential function whose width is determined by the standard deviation of the Gaussian pdf. Thus, for a given value of μ, fewer and fewer fringes are observed as σ increases.

Finally, it should be pointed out that Eqs. (1) - (5) do not accurately describe the intensity near the origin of the transform plane. Since a significant portion of the incident light is undiffracted by the hologram, a narrow, intense distribution of light (which is the Fourier transform of the aperture of the optical system) will be observed at the origin of the transform plane.

A method of obtaining 1-dimensional displacement and velocity distributions from intensity measurements in the transform plane of a double-exposure hologram

An expression for the intensity in the transform plane of a double-exposure far-field hologram is given by Eq. (4) where it is assumed that the particle displacements can be characterized by a 1-dimensional pdf $p(s_1)$. Clearly, $p(s_1)$ is the desired quantity; the goal is to develop a means of obtaining it from the measured intensity data $\langle I_F(u,v)\rangle$. The first step in obtaining $p(s_1)$ is to divide both sides of Eq. (4) by $I_0(u,v)$, yielding

$$I'(u) = \frac{\langle I_F(u,v)\rangle}{I_0(u,v)} = 1 + \int_{-\infty}^{\infty} p(s_1)\cos(\frac{2\pi u s_1}{\lambda f})\,ds_1. \qquad (6)$$

For the present discussion it will be assumed that $I_0(u,v)$ is known; a method of obtaining this quantity is described in this paper. It should be recalled that $I_0(u,v)$ contains a zone lens term (i.e., $\cos^2(\cdot)$ in Eq. (3)) which exhibits numerous zeros in the u,v-plane. Thus there appears to be a problem in dividing Eq. (4) by $I_0(u,v)$ due to the zeros of the zone lens. In practice, however, there is no difficulty since the zone lens may effectively be removed from the transform pattern by increasing its frequency (by increasing the object-to-hologram separation z) beyond the resolution limit of the detector used to measure $\langle I_F(u,v)\rangle$. Alternatively, off-axis holography may be used to eliminate the zone lens entirely.[15]

The density function may be obtained from Eq. (6) by taking the Fourier transform of $I'(u)$, i.e.,

$$F\{I'(u)\} = \int_{-\infty}^{\infty} I'(u)\exp[-i2\pi u\alpha]du\ , \qquad (7)$$

where α is the transform variable. Substituting the right-hand side of Eq. (6) into the above expression yields

$$F\{I'(u)\} = \delta(\alpha) + \frac{\lambda f}{2}p(-\lambda f\alpha) + \frac{\lambda f}{2}p(\lambda f\alpha)\ , \qquad (8)$$

where $\delta(\alpha)$ is the Dirac delta function. The above result indicates that the desired pdf can be obtained by properly processing intensity data measured in the transform plane. It should be noted that the pdf $p(\cdot)$ appears twice in the above expression (i.e., once with the argument $+\lambda f\alpha$ and once with $-\lambda f\alpha$) as a result of the 180° ambiguity in determining the direction of particle motion from a double-exposure hologram.

Measuring 2-dimensional velocity and displacement distributions

If the particle motion is characterized by a 2-dimensional distribution of displacements (where the particle motion is confined to a plane parallel to the hologram plane), the displacement information is displayed in the optical transform plane in accordance with Eq. (2). Thus it appears that a 2-dimensional distribution of

displacements may be measured by an appropriate generalization of the 1-dimensional data processing method described in the previous section. This generalization would, in fact, be possible if the quantity $\langle I_F(u,v)\rangle$ in Eq. (2) could be measured accurately throughout the transform plane. It must, however, be remembered that the strong component of undiffracted light prevents us from obtaining $\langle I_F(u,v)\rangle$ in the vicinity of the origin of the transform plane. Since $\langle I_F(u,v)\rangle$ cannot be determined near $u = v = 0$, the two-dimensional pdf $p(s_1,s_2)$ cannot be accurately obtained in general. Of course, this problem does not exist in the 1-dimensional case since only a 1-dimensional scan of the intensity pattern in the transform plane is required to compute $p(s_1)$. This scan may be taken at some distance away from the origin; hence, the undiffracted light does not cause any serious difficulties.

Two-dimensional velocity and displacement distributions can, however, be measured when the horizontal and vertical components of displacement are statistically independent. In this case, the joint density function $p(s_1,s_2)$ may be expressed as a product of the marginal density functions,[16] i.e., $p(s_1,s_2) = p_1(s_1)p_2(s_2)$. Substituting the above expression into Eq. (2) yields, after dividing both sides of Eq. (2) by $I_0(u,v)$,

$$I'(u,v) = 1 + \int_{-\infty}^{\infty}\int p_1(s_1)p_2(s_2)\cos\left[\frac{2\pi}{\lambda f}(us_1 + vs_2)\right] ds_1 ds_2 . \qquad (9)$$

If the intensity pattern is sampled along a line parallel to the u-axis and at a distance v_0 from the origin, the above expression becomes

$$I'(u,v) = 1 + \int_{-\infty}^{\infty}\int p_1(s_1)p_2(s_2)\cos\left[\frac{2\pi}{\lambda f}(us_1 + v_0 s_2)\right] ds_1 ds_2 . \qquad (10)$$

(By scanning the transform pattern away from the origin, the problems associated with the undiffracted component of light are virtually eliminated.) Transforming the above equation with respect to the variable u yields

$$F\{I'(u,v)\} = \delta(\alpha) + \frac{\lambda f}{2}[p_1(-\lambda f\alpha) + p_2(\lambda f\alpha)] \int_{-\infty}^{\infty} p_2(s_2)\cos\frac{2\pi v_0 s_2}{\lambda f} ds_2 , \qquad (11)$$

where α is the transform variable. Since v_0 is a constant, the integral in Eq. (11) evaluates to a constant. Thus the above expression indicates that the marginal density function may be determined (to within a constant factor) from data obtained in a 1-dimensional scan of the intensity pattern. The ambiguity introduced by the unknown constant factor may be resolved by using the fact that the area under the pdf is equal to unity by definition. Finally, $p_2(s_2)$ may be determined in a similar fashion by processing the data obtained from a scan parallel to the v-axis at a distance u_0 from the origin.

Data acquisition

A system consisting of a TV camera, an image digitizer and a computer (PDP-11/23) was used to acquire and process the optical data (i.e., the intensity distribution in the transform plane of the doubly exposed hologram). The digitizer (Video Frame Store 274 D, manufactured by Colorado Video, Inc.) converts a given frame of analog video information to a digitized image consisting of 512 x 512 pixels with 256 gray-levels. The digitized image is retained in the memory of the frame store and the PDP-11/23 may then be used to access any desired pixel or group of pixels from the frame store. Once the required data is in the computer, it is processed to yield the particle displacement information.

Experimental results

It would be desirable to record a hologram of a particle sample for which the velocity distribution of the particles is known in advance since this hologram may then be used as a test input to the optical-digital (or hybrid) system described above. The particle displacement information determined by the hybrid system may be compared to the known displacements, thereby indicating whether or not the system is performing as expected. Unfortunately, it is difficult in practice to produce a double-exposure hologram of a dynamic sample for which the distribution of particle displacements is known *a priori*. As a result, a method for simulating a double-exposure hologram was developed. The first step in producing such a hologram was to plot a random array of dots using a graphics plotter operating under computer control. The random array consisted of dot-pairs which were uniformly distributed over the plotting area; the spacing between the

dots comprising a given dot-pair was determined by a Gaussian random number generator to simulate a Gaussian distribution of displacements. The random array was then photo-reduced; the resulting black discs (~ 40μm in diameter) on the otherwise transparent photographic plate form diffracting objects which simulate particles. (A similar procedure for producing a random array of dots has recently been reported in connection with the study of fringe visibility in speckle velocimetry.[17]) A far-field hologram of the simulated particles was then recorded to provide a test input to the hybrid system. Results obtained by using far-field holograms of random arrays are presented in Figs. 2-9 and are described below.

The intensity profile I_F in the transform plane of a hologram of a random array of discs is shown in Fig. 2a; the intensity profile was obtained by using the TV camera and image digitizer as described above. (An Argon-ion laser operating at 5145 Å was used in recording the hologram and in forming the optical Fourier transform.) In this example, the separation between disc-pairs is characterized by a Gaussian pdf where $\mu = 460\ \mu m$ and $\sigma = 30\mu m$. The measured intensity in Fig. 2a is plotted on a relative scale of 0 to 255, corresponding to the 256 gray-levels provided by the image digitizer. Furthermore, the intensity pattern was sampled at 128 intervals along a direction perpendicular to the fringe pattern. Thus, the position along the horizontal axis is expressed in terms of integers ranging from 0 to 127 where each integer corresponds to a particular pixel; the actual width of the diffraction pattern represented by Fig. 2a is approximately 14mm.

It should be recalled that the first step in obtaining the required density function from the measured intensity profile is to determine the particle-size-dependent envelope I_0 so that the quotient I_F/I_0 may be evaluated. The envelope may be obtained directly from the measured intensity data by recognizing that the envelope itself is rather slowly varying while the term carrying the velocity information is rapidly varying. Hence, if the measured intensity profile is passed through a suitable low-pass filter, the output would be the envelope I_0. The filtering operation is demonstrated in Figs. 2b - 3b. The first step is to evaluate the fast Fourier transform (FFT) of the measured intensity profile; Fig. 2b shows the magnitude of the FFT as a function of the discrete transform variable n. The origin of the frequency axis in Fig. 2b was shifted from n=0 to n=64 to produce a symmetrical plot, thus the low frequency information is centered about the point n=64. The filtering is performed by setting the magnitude of the FFT to zero for all points except those in an interval about n=64; the values of the FFT within this interval remain unchanged (see Fig. 3a). The inverse transform of the filtered data is then computed, yielding the envelope function (Fig. 3b).

The next step in determining the required pdf is to compute I_F/I_0; the result of performing this division is shown in Fig. 4a. Since I_F and I_0 assume small values near n=0 and n=127, small fluctuations in I_F will be greatly amplified when I_F/I_0 is computed (see Fig. 4a). To obtain accurately the pdf that characterizes the distribution of particle displacements, it is necessary to remove these random fluctuations by setting I_F/I_0 to unity over the appropriate intervals (see Fig. 4b). Computing the FFT of the curve shown in Fig. 4b then yields the required pdf (Fig. 5a); the portion of the curve in Fig. 5a that represents the density function is redrawn in Fig. 5b where the peak value of this curve is normalized to unity for convenience. To compare the shape of the experimentally obtained curve with the theoretical curve, the theoretical Gaussian pdf was plotted so that its peak value coincides with that of the curve obtained experimentally (see Fig. 5b). It is observed that the agreement betwen the two curves is quite good.

The results shown in Figs. 6-8 were also obtained by applying a far-field hologram of a random array of discs as input to the hybrid system and processing the data as outlined above. In this case, the separation between disc-pairs was again determined by a Gaussian random number generator but with $\mu = 490\mu m$ and $\sigma = 70\mu m$. The relatively large value used for σ was selected to demonstrate the ability to measure a relatively wide distribution. The measured intensity profile I_F is shown in Fig. 6a and a plot of I_F/I_0 is given in Fig. 6b. (The filtering operation is not shown here because it is very similar to that shown in the previous example.) Since σ is large in comparison to that of the previous example, the interval over which displacement-dependent fringes are observed is relatively small. (Clearly, this result is expected from Eq. (5).) Outside of this interval, random fluctuations primarily due to speckle noise are observed. As demonstrated in Figs. 7 and 8, it is necessary to remove the fluctuations that lie outside the aforementioned interval to obtain the desired pdf accurately. In Fig. 7a, a significant portion of the fluctuations were removed and, as a result, the computed pdf is in good agreement with the theoretical pdf (see Fig. 7b). In Fig. 8a, a relatively small portion of the random fluctuations were removed and the pdf that results does not agree very well with the theoretical pdf.

In the case of a 2-dimensional distribution, it was indicated that the marginal pdfs may be obtained if the orthogonal components of displacement are statistically independent. That is, taking two orthogonal scans in the transform plane and processing

the data as outlined above will yield the marginal density functions. To demonstrate, a random array of opaque discs was once again used to simulate particles in motion. In this case, however, the displacement between the discs which comprise a typical disc-pair was random in two dimensions; i.e., the horizontal and vertical components of displacement were both determined by a Gaussian random-number generator. The mean and standard deviation of the horizontal component of displacement is denoted by μ_1 and σ_1, respectively. Similarly, the parameters for the vertical component are given by μ_2 and σ_2 where $\mu_2 = \mu_1 = 450\mu m$ and $\sigma_2 = \sigma_1 = 35\mu m$. The resulting system output is given in Fig. 9 which shows the measured pdf along with the theoretical result. It is observed that the agreement betwen the two curves is quite good.

Finally, the velocity distribution of particles falling in water was measured to demonstrate that the hybrid system for automated readout may be applied in practice. The distribution was obtained by allowing 79μm corn pollen particles to fall in water, and a chopped cw laser beam (Argon-ion operating at 5145 Å) was then used to record a double-exposure hologram of the particle sample. After measuring the intensity profile in the transform plane of the hologram and processing the data in the prescribed manner, the density function shown in Fig. 10 was obtained. It is observed that the distribution is Gaussian-like with a mean speed of approximately 2.5 mm/sec.

Conclusions

Double-exposure holography together with the hybrid readout system offers a fast and reliable method for measuring particle velocity distributions. In fact, if a suitable hologram can be recorded in real time, the entire velocity measurement process can, in principle, be carried out in real time. While the displacement and velocity information is readily obtained in the transform plane of the hologram, the spatial information of the individual particles is effectively lost. However, the reconstructed holographic image of the sample volume can be examined to yield the individual particle locations, if necessary.

Finally, it should be noted that if the particle displacements are characterized by a wide pdf (i.e., σ is large), displacement-dependent fringes will not be observed in the transform plane (see Eq. (5)). Thus, the techniques described in this paper cannot be used to determine the distribution of displacements. However, it should be possible to handle relatively wide distributions by dividing the hologram into sections. Each section may then be analyzed individually, presuming that the distribution represented by each section is sufficiently narrow.

References

1. Silverman, B. A., B. J. Thompson and J. H. Ward, "A Laser Fog Disdrometer," J. Appl. Meterology, Vol. 3, No. 6, pp. 792-801. 1964.
2. Thompson, B. J., G. B. Parrent, J. H. Ward and B. Justh, "A Readout Technique for the Laser Fog Disdrometer," J. Appl. Meterology, Vol. 5, No. 3, pp. 343-348. 1966.
3. Thompson, B. J., "Holographic Particle Sizing Techniques," J. Phys. E., Vol. 7, pp. 781-788. 1974.
4. Trolinger, J. D., "Particle Field Holography," Opt. Eng., Vol. 14, No. 5, pp. 383-392. 1975.
5. Thompson, B. J. and P. Dunn, "Advances in Far-Field Holography -- Theory and Applications," Proc. SPIE, Vol. 215, pp. 102-111. 1980.
6. Thompson, B. J., "Holographic Methods of Dynamic Particulate Measurements -- Current Status," 15th International Congress on High Speed Photography and Photonics, Lincoln L. Endelman, Editor, Proc. SPIE 348, pp. 626-632. 1982.
7. Grabowski, W., "Measurement of the Size and Position of Aerosol Droplets Using Holography," Optics and Laser Technology, Vol. 15, No, 4, pp. 199-205. 1983.
8. Vikram, C. S. and M. L. Billet, "Far-Field Holography at Non-image Planes for Size Analysis of Small Particles," Appl. Phys. B, Vol. 33, pp. 149-153. 1984.
9. Slimani, F., G. Grehan, G. Govesbet and D. Allano, "Near-Field Lorentz-Mie Theory and its Application to Microholography," Appl. Opt., Vol. 23, No. 22, pp. 4140-4148. 1984.
10. Prikryl, I. and C. M. Vest, "Holographic Imaging of Semitransparent Droplets or Particles," Appl. Opt., Vol. 21, No. 14, pp. 2541-2547. 1982.
11. Bexon, R., J. Gibbs and G. D. Bishop, "Automatic Assessment of Aerosol Holograms," J. Aerosol Sci., Vol. 7, pp. 397-407. 1976.
12. Payne, P. R., K. L. Carder and R. G. Steward, "Image Analysis Techniques for Holograms of Dynamic Oceanic Particles," Appl. Opt., Vol. 23, No. 2, pp. 204-210. 1984.
13. Ewan, B. C. R., "Holographic Particle Velocity Measurement in the Fraunhofer Plane," Appl. Opt., Vol. 18, No. 5, pp. 623-626. 1979.
14. Ewan, B. C. R., "Particle Velocity Distribution Measurement by Holography," Appl. Opt., Vol. 18, No. 18, pp. 3156-3160. 1979.

15. Malyak, P. and B. J. Thompson, "Particle Displacement and Velocity Measurement Using Holography," Opt. Eng., Vol. 23, No. 5, pp. 567-576. 1984.
16. Papoulis, A., Probability, Random Variables and Stochastic Processes, McGraw-Hill, 1965.
17. Hinsch, K., W. Schipper and D. Mach, "Fringe Visibility in Speckle Velocimetry and the Analysis of Random Flow Components," Appl. Opt., Vol. 23, No. 24, pp. 4460-4462. 1984.

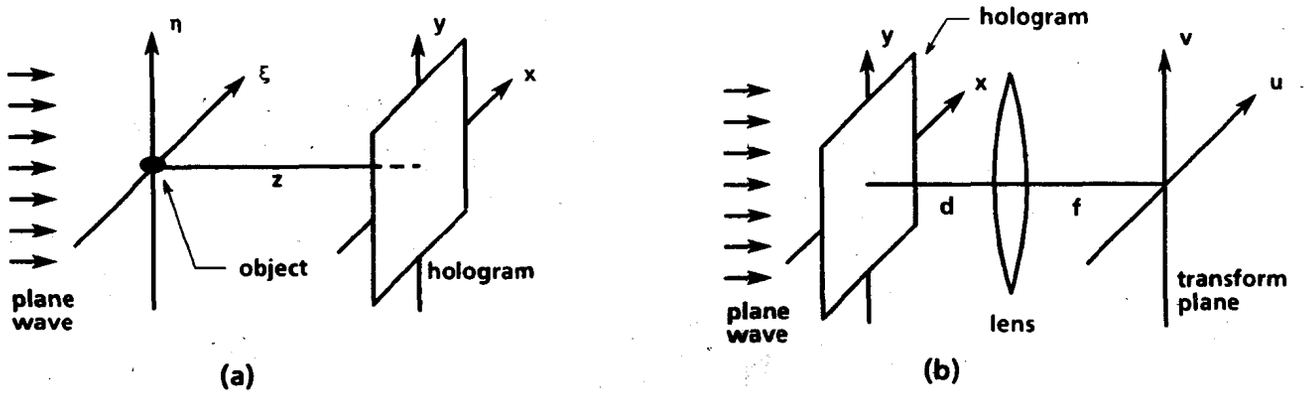

Fig. 1. (a) Hologram recording geometry. (b) Geometry for forming the optical Fourier transform.

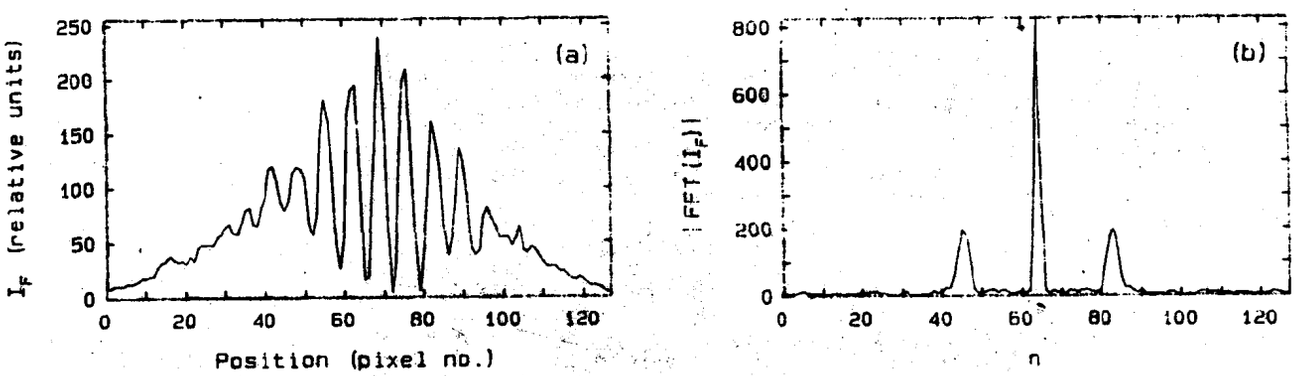

Fig. 2. (a) Plot of the intensity profile in the transform plane of a far-field hologram of a random array of opaque discs. The separation between disc-pairs is characterized by a Gaussian probability density function (pdf); μ = 460μm and σ = 30μm. (b) Magnitude of the FFT of the intensity profile vs. the discrete transform variable n.

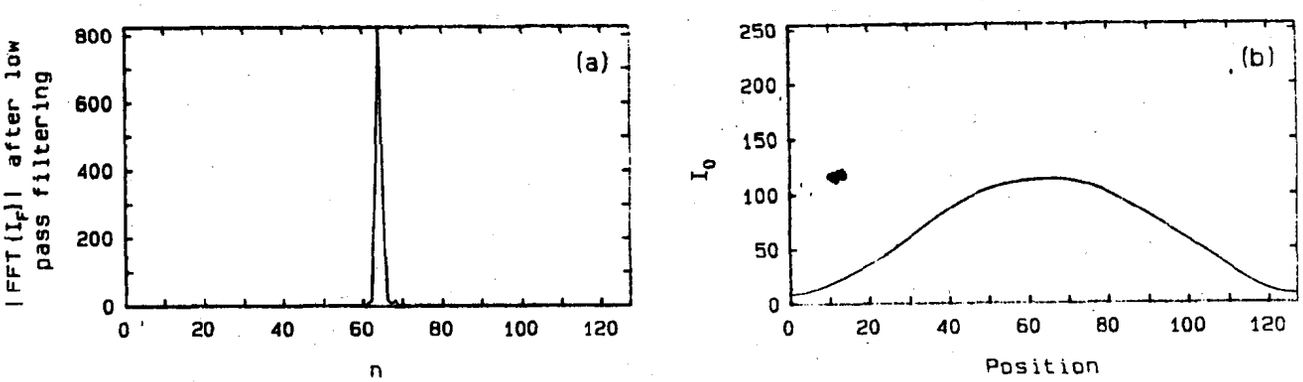

Fig. 3. (a) Plot of $|FFT\{I_F\}|$ vs. n after low pass filtering. (b) The envelope function I_0 is obtained by computing the inverse FFT of the data in (a).

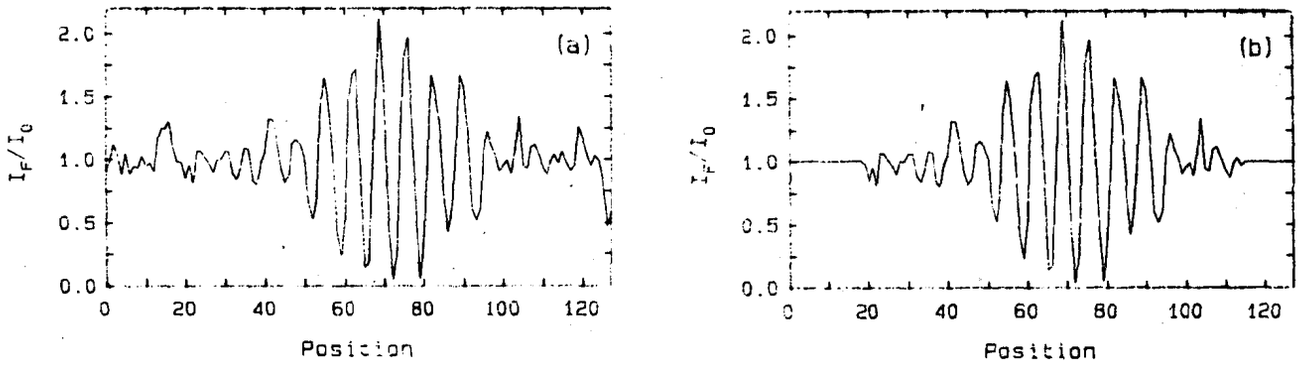

Fig. 4. (a) Plot of I_F/I_0 vs. position. (b) Same as (a) except the random fluctuations at the left and right portions of the curve were removed by setting I_F/I_0 equal to unity.

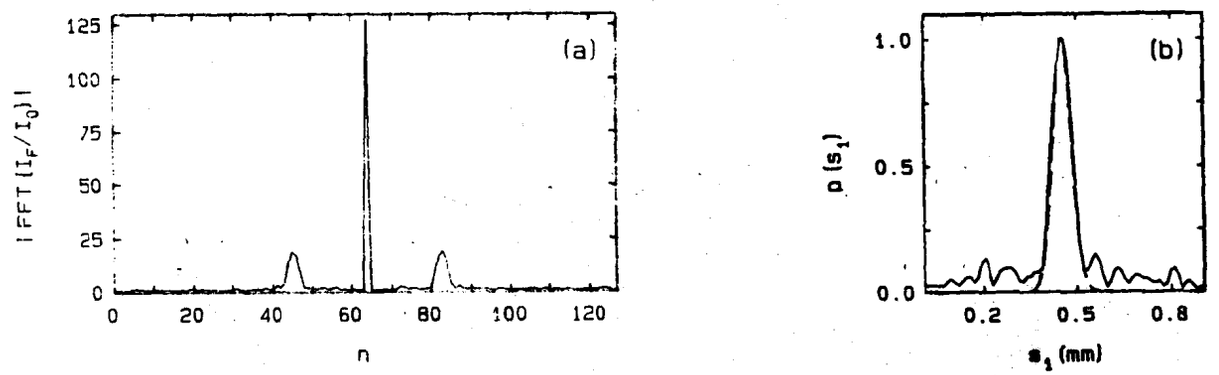

Fig. 5. (a) Magnitude of $FFT\{I_F/I_0\}$ vs. the discrete transform variable n. (b) Plot of the computed (____) density function and the theoretical (----) density function vs. displacement.

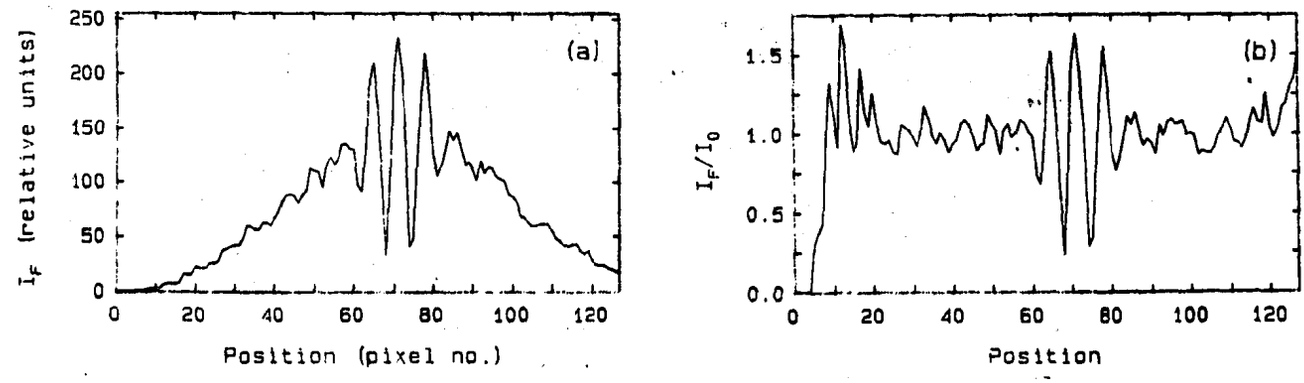

Fig. 6. (a) Plot of the intensity profile in the transform plane of a far-field hologram of a random array of opaque discs. The separation between disc-pairs is characterized by a Gaussian pdf; μ = 490μm and σ = 70μm. (b) Plot of the intensity profile, I_F, divided by the envelope I_0.

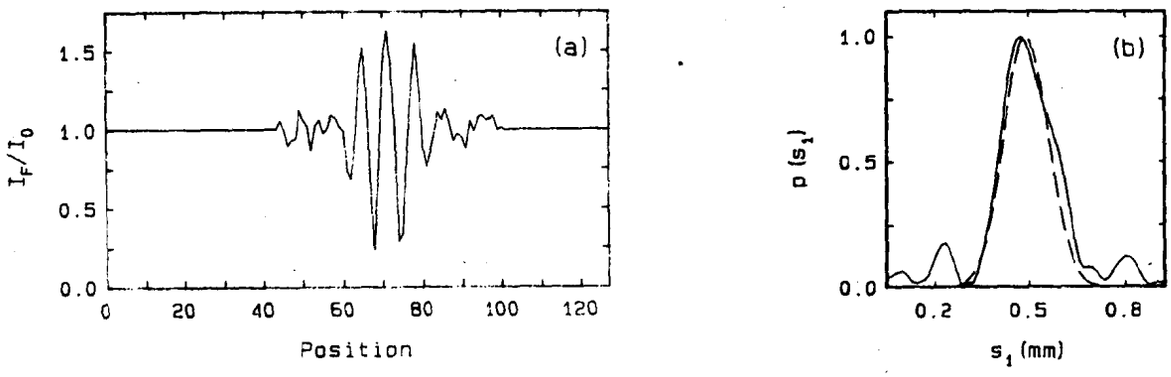

Fig. 7. (a) Same as 6b except the random fluctuations at the left and right portions of the curve were removed. (b) Plot of the computed (____) density function and the theoretical (----) density function vs. displacement.

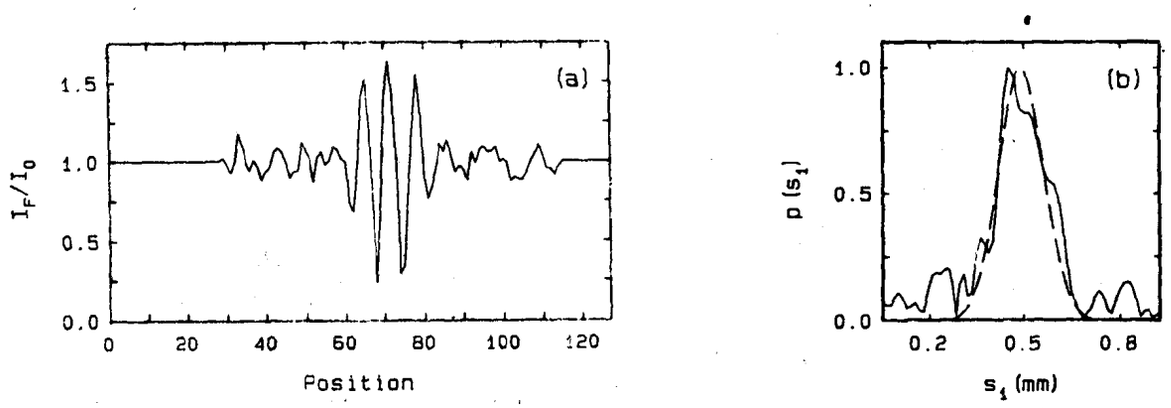

Fig. 8. (a) Same as 6b except a relatively small portion of the random fluctuations at the left and right extremes of the curve were removed. (b) Plot of the computed (____) density function and the theoretical (----) density function vs. displacement.

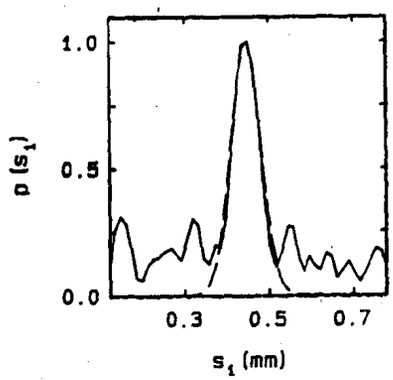

Fig. 9. Plot of the computed (____) marginal density function and the theoretical (----) density function vs. displacement. In this example, the separation between the disc-pairs that comprise the random array is characterized by a 2-dimensional Gaussian pdf where $\mu_1 = \mu_2 = 450\mu m$ and $\sigma_1 = \sigma_2 = 35\mu m$.

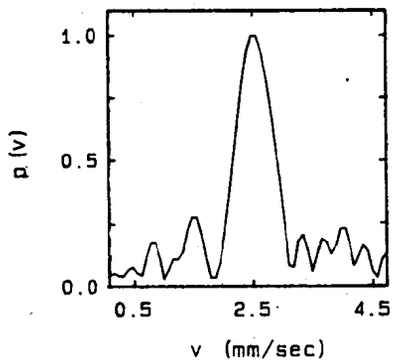

Fig. 10. Plot of the experimentally obtained density function which characterizes the velocity distribution of 79 μm pollen particles falling in water.